Comparison of Theoretical and Absolute Experimental Fully-Differential Cross Sections for Ion-Atom Impact-Ionization

D. Madison[1], M. Schulz[1], S. Jones[1], M. Foster[1], R. Moshammer[2], and J. Ullrich[2]

[1]Laboratory for Atomic, Molecular and Optical Research, University of Missouri-Rolla, Rolla, MO, USA, 65409
[2]Max-Planck-Institut für Kernphysik, Saupfercheckweg 1, D-69117 Heidelberg Heidelberg, Germany

Abstract

We report fully differential cross section (FDCS) calculations and absolute measurements for ion-atom impact ionization. Using the COLTRIMS (cold target recoil ion momentum spectroscopy) method, we have obtained absolute FDCS both in the scattering plane as well as out of the scattering plane for 100 MeV/amu C^{6+} ionization of helium. FDCS results are presented for different projectile scattering angles and ejected-electron energies. The measurements are compared with a theoretical calculation employing an asymptotically exact three-body final-state wavefunction that contains all active two-particle subsystem interactions to infinite order in perturbation theory. For the active electron, a Hartree-Fock bound-state wavefunction is used for the initial state and numerical continuum-state eigenfunctions of a Hartree-Fock potential for the ion are used for the final state. In the scattering plane, these theoretical results are in very good agreement with experiment for small and intermediate momentum transfer. However, some significant discrepancies are found for large momentum transfer and outside the scattering plane. These discrepancies disappear upon comparison with successively less-differential cross sections.

1. Introduction

Fully differential cross sections (FDCS) have been studied for electron-impact ionization of atoms for over three decades and significant theoretical progress has been made particularly in the last twenty years. For the case of electron-impact ionization of hydrogen and helium, experiment and theory are in reasonably good accord in the scattering plane for energies well above threshold (Jones and Madison 1998 and 2000, Bray *et al*. 2001). The important remaining questions are mainly concerned with near-threshold ionization of hydrogen and this problem has recently attracted intense interest and controversy (Bencze and Chandler 1999, Bray 1999, Stelbovics 1999, Rescigno *et al*. 1999, Bray 2000, Madison *et al*. 2000, Bray *et al*. 2001 and 2002, Baertschy 2002). The situation is much different for electron-impact ionization of the heavier inert gases where experiment and theory are not in good accord for incident electron energies below about 100 eV (Haynes and Lohmann 2001a and 2001b, Biava *et al*. 2002). It should be noted that the different theoretical methods discussed in the above cited papers all give essentially identical total ionization cross sections. Discrepancies appear only when their respective differential cross sections are compared. Thus the importance of differential cross section measurements cannot be overemphasized. In the present COLTRIMS (cold target recoil ion momentum spectroscopy) experiment, all ionizing events are determined in full coincidence which means that the total cross sections and all differential cross sections are obtained simultaneously in a single experiment.

For the case of heavy-particle impact ionization, experimental technology for measuring FDCS was not developed until 1994 (Moshammer et al. 1994). However, it took another seven years until the first measurements were actually reported (Schulz *et al*., 2001). In that paper, FDCS measurements were presented for 100 MeV/amu C^{6+} ionization of helium for different energies of the ejected electron and different angles of the scattered projectile. It was found that the shape of the FDCS in the scattering plane was very similar to electron scattering cross sections for comparable kinematical conditions with a binary peak near the momentum transfer direction and a recoil peak in the opposite direction. In the scattering plane, the shape of the experimental data was in good

agreement with both the first Born approximation (FBA) and the three-Coulomb-wave (3C) results as would be expected for a high-energy collision. The unexpected observation was that the experimental data out of the scattering plane exhibited structure that was not well reproduced by theory. This observation suggested that effects not contained in the theories might be important out of the scattering plane.

We have now placed the experimental data on an absolute scale and we have improved the theory. The 3C code that was previously used was restricted to approximating the final-state wavefunctions for both the scattered projectile and ejected electron as hydrogenic Coulomb waves for some effective charge. Consequently, the standard helium effective charge of 1.69 was used (we will call these results the 3C-169). Although this effective charge is probably reasonable for distances close to the nucleus, it is asymptotically incorrect. It has been well established for electron scattering that it is important to use wavefunctions that are asymptotically correct. Therefore, a much better approach, particularly for the ejected electron, would be to use a wavefunction calculated from the Hartree-Fock static potential for the residual helium ion since this wavefunction would have the proper behavior both close to the nucleus as well as asymptotically (Madison and Shelton 1973, Manson *et al*. 1975, Fainstein *et al*. 1994, Gulyás *et al*., 1995, Stolterfoht *et al*. 1997, Gulyás and Fainstein 1998). Here we will report the results of such a calculation.

The overwhelming majority of both perturbative and non-perturbative theoretical descriptions of ion-atom ionization use a straight-line trajectory for the projectile and ignore the internuclear interaction (see review by Fainstein *et al*. 1991 and references therein, Stolterfoht *et al*. 1997, Fiol *et al*. 2001). This impact parameter treatment in conjunction with the neglect of the internuclear interaction at high impact energies is an excellent example of the right way to do theoretical physics if one is interested in electron spectra (Moshammer *et al*. 1999) since the goal of theory should be to explain physical observations using the *minimum* amount of necessary physics. Nevertheless, these approximations are not valid for fully differential cross sections (or any cross section differential in projectile scattering angle – see Salin 1989, Fukuda *et al.* 1991a and

1991b, Fang and Reading 1991, Rodríguez and Barrachina 1998, Moshammer *et al*. 2001, Fiol *et al*. 2001, Schulz *et al*. 2002). Therefore, in the present work, the internuclear interaction is included and the projectile motion is treated fully quantum mechanically.

2. Theory

We consider ionization of atoms in the ground state by incident charged particles of arbitrary charge and mass. For this case, one needs to use the center-of-mass (CM) system. The ionization event is regarded as an effective three-body process – the incident projectile with mass M_p and charge Z_p, the ejected electron, and the residual ion with mass M_I and asymptotic charge of +1. In the CM system, all quantities can be expressed in terms of the Jacobi coordinates (**r**,**R**), where **r** is the coordinate of the atomic electron relative to the center of mass of the ion and **R** is the position of the projectile relative to the center of mass of the ion plus electron (see fig. 1). For all practical purposes, both the laboratory and Jacobi coordinate systems will have their origins at the nucleus of the target, which we assume is at rest. In the CM coordinate system, the fully differential cross section (FDCS) is given by (Bethe 1930, Inokuti 1971, Berkadar et al. 1993)

$$\frac{d^3\sigma}{d\Omega_p d\Omega_e dE_e} = N_e\,(2\pi)^4\,\mu_{Ie}\,\mu_{PA}^2\,\frac{k_f\,k_e}{k_i}\left|T_{fi}\right|^2 \qquad (1)$$

Here N_e is the number of identical electrons in the atomic shell which is ionized and the reduced masses are given by

$$\mu_{Ie} = \frac{M_I}{M_I+1} \approx 1$$
$$\mu_{PA} = \frac{M_P(M_I+1)}{M_P+M_I+1} \approx \frac{M_P M_I}{M_P+M_I} \qquad (2)$$

The projectile momentum $\mathbf{K}_i\,(\mathbf{K}_f)$ is the CM initial (final) momentum conjugate to $\mathbf{R}$

$$\begin{aligned}\mathbf{K}_i &= \mu_{PA}\mathbf{V}_0 \\ \mathbf{K}_f &= \mu_{PA}\mathbf{V}_f\end{aligned} \tag{3}$$

with $\mathbf{V}_0\,(\mathbf{V}_f)$ being the initial (final) velocity of the projectile relative to the atomic center of mass. If E_o is the incident energy of the projectile (in the lab frame) and ΔE is the energy loss of the projectile, we have

$$\begin{aligned}V_0 &= \sqrt{\frac{2E_0}{M_P}} \\ V_f &= \sqrt{V_0^2 - \frac{2\Delta E}{\mu_{PA}}}\end{aligned} \tag{4}$$

The momentum of the ejected electron is

$$\mathbf{k}_e = \mu_{Ie}\mathbf{v}_e \tag{5}$$

where $\mathbf{v}_e$ is the velocity of the ejected electron with respect to the center of mass of the ion. In Eq. (1), the projectile is scattered into solid angle $d\Omega_P$ relative to the incident beam direction $\hat{K}_i$ and the atomic electron is ejected into solid angle $d\Omega_e$ with energy E_e. Consequently, the FDCS of Eq. (1) is really a five-fold differential cross section (four angles and one energy). The flux factor in Eq. (1) assumes that all continuum waves are normalized to a delta function in momentum. The T-matrix is given by

$$T_{fi} = \left\langle \Psi_f^-(\mathbf{R},\mathbf{r}) \middle| H - H_0 \middle| \Phi_i(\mathbf{R},\mathbf{r}) \right\rangle \tag{6}$$

Where H is the full Hamiltonian for the system, Ψ_f is the exact final-state three-body wavefunction which is an eigenfunction of H and

$$H_0\left|\Phi_i(\mathbf{R},\mathbf{r})\right\rangle = E\left|\Phi_i(\mathbf{R},\mathbf{r})\right\rangle \tag{7}$$

with E the total energy. If we represent the ion by a Hartree-Fock (HF) spherically symmetric potential U_{ion}, the full Hamiltonian will have the form

$$H = T_P + T_e + V_{Pe} + Z_P\, U_{ion} + Z_e\, U_{ion} \tag{8}$$

where $T_P\,(T_e)$ is the kinetic energy operator for the projectile (electron), V_{Pe} is the projectile-electron interaction and the charge of the electron $Z_e = -1$. The initial-state Hamiltonian is

$$H_0 = T_P + T_e + Z_e\, U_{ion} \tag{9}$$

As a result, the initial-state wavefunction will be a product of a plane wave $PW_i\,(\mathbf{R})$ for the projectile and a bound-state HF wavefunction for the electron $\psi_i\,(\mathbf{r})$. In principle, the bound-state wavefunction should be calculated as an eigenfunction of U_{ion}. In practice we use the bound-state Hartree-Fock wavefunction which was used in the calculation of U_{ion}. Consequently

$$T_{fi} = \left\langle \Psi_f^-(\mathbf{R},\mathbf{r}) \right| V_{Pe} + Z_P\, U_{ion} \left| \psi_i(\mathbf{r})\, PW_i(\mathbf{R}) \right\rangle \tag{10}$$

No approximations (to the effective three-body problem) have been made to this point. For a practical calculation, one has to approximate the exact final-state wavefunction. For the case of ionization of hydrogen by electron impact, Brauner, Briggs and Klar (1989) demonstrated that it was necessary to pick a final-state wavefunction that satisfied the exact three-body boundary conditions in order to get good agreement with experiment for intermediate impact energies. For hydrogen, the resulting wavefunction, known as the 3C wavefunction, is a product of two Coulomb waves and a Coulomb distortion factor. This wavefunction contains the Coulomb interaction for each two-particle subsystem of the three particles. While it is reasonable to use a Coulomb wave for the

fast projectile with Z_{eff} = 1, a Coulomb wave is likely to be unreliable for a slow ejected electron. Consequently, the final-state wavefunction is approximated as

$$\Psi_f^-(\mathbf{R},\mathbf{r}) = CW_P^-(\mathbf{R})\,\chi_e^-(\mathbf{r})C_{Pe}^-(\mathbf{R},\mathbf{r}) \tag{11}$$

where CW_P is a Coulomb wave for the projectile (Z_{eff} = 1 for the ion), χ_e is the wavefunction for the ejected electron, and $C_{Pe}(\mathbf{R},\mathbf{r})$ is the Coulomb distortion factor for the projectile-electron sub-system. With these approximations, the T-matrix we evaluate for ionization of helium is

$$T_{fi} = \left\langle CW_P^-(\mathbf{R})\,\chi_e^-(\mathbf{r})C_{Pe}^-(\mathbf{R},\mathbf{r})\right|\, V_{Pe} + Z_P\,U_{ion}\left|\psi_i(\mathbf{r})\,PW_i(\mathbf{R})\right\rangle \tag{12}$$

We have set CW_P to a Coulomb wave for charge unity to satisfy the asymptotic boundary conditions and in the same spirit we set the interaction of the projectile with the ion as

$$Z_P\,U_{ion} = \frac{Z_P}{R} \tag{13}$$

Finally, the ejected-electron wavefunction χ_e is a numerical solution of the Schrödinger equation

$$(T_e + Z_e\,U_{ion} - \frac{k_e^2}{2\mu_{Ie}})\,\chi_e^- = 0 \tag{14}$$

Similar to the projectile wavefunction, χ_e is asymptotically in a Coulomb field for charge unity. The numerical solutions of the Schrödinger equation (14) contain the static electron-ion interaction to infinite order in perturbation series. Since the initial state of the ejected electron is a HF wavefunction and the final state is a static HF wavefunction, we call our results 3C-HF. We evaluate the amplitude (10) through a full 6-dimensional integration without making any additional approximations about the trajectory of the heavy projectile.

In the next section we will also show first Born approximation results. There are many different variations of the FBA depending on the choice of initial and final state wavefunctions for the active electron and depending on whether or not the projectile-nuclear interaction is included in the interaction operator. The FBA T-matrix we evaluate is

$$T^{FBA-HF} = \left\langle PW_P(\mathbf{R})\,\chi_e^-(\mathbf{r}) \,\middle|\, V_{Pe} + Z_P\,U_{ion} \middle| \psi_i(\mathbf{r})\,PW_i(\mathbf{R}) \right\rangle \qquad (15)$$

Hence, our first Born results represent the limit of the 3C-HF calculation when the projectile wavefunction in the final state is a plane wave and the final-state projectile-electron interaction is ignored. Consequently we label this approximation as FBA-HF. For orthogonal initial and final active-electron wavefunctions (which is nearly the case here), the projectile-ion interaction makes not contribution to the T-matrix. It is important to note that the initial- and final-state wavefunctions for the active electron are the same in both the FBA-HF and 3C-HF. Consequently, even though this is a first-Born approximation for the projectile, the static electron-ion interaction is contained to infinite order in perturbation series.

3. Results

The absolute normalization of the experimental data was performed by exploiting the large acceptance of the spectrometer as follows: The experiment is not only kinematically complete but, in addition, simultaneously records in a triple coincidence all electrons with energies between 0 and 50 eV, all recoiling ions with momenta smaller than 10 a.u. as well as all the scattered projectiles. Thus, a large part of the total cross section is measured simultaneously and the integrated total number of coincident recoiling He^+ ions, for instance, corresponds to a well defined part of the total single ionization cross section, namely the single differential ionization cross sections (SDCS) as a function of the ionized electron energy integrated from 0 to 50 eV. Rudd et al. (1985, 1992) demonstrated that the present FBA-HF is reliable for calculating the SDCS

integrated over ejected electron energy. Consequently, the integrated recoil spectrum and thereby subsequently all measured FDCS were normalized to 1.29 x 10^{-17} cm^2 which is the FBA-HF results integrated over the same energy range. It should be kept in mind that any FDCS projected out of the complete data set are automatically normalized relative to each other and are on an absolute scale by the above procedure.

3.1 Scattering Plane

The fully differential cross sections are differential in the solid angle of observation for the scattered projectile, differential in the solid angle of observation for the ejected electron and differential in the energy of the ejected electron (five fold differential). The coordinate system we use has the z-axis parallel to the incident beam direction, the y-axis perpendicular to the scattering plane and directed up, and the x-axis in the scattering plane directed left of the beam direction for an observer above the scattering plane looking along the beam propagation (see fig. 2). The projectile is scattered to the left (in the positive x-direction) which causes the binary electrons to be scattered to the right in the negative x-direction. The momentum transfer direction $\mathbf{Q} = \mathbf{K}_i - \mathbf{K}_f$ is very close to 90° which would correspond to the negative x-direction. We use standard spherical coordinates with θ_e being measured relative to the beam direction, $\phi_e = 0$ corresponds to the half plane containing the positive x-axis and $\phi_e = \pi$ corresponds to the half plane containing the negative x-axis. The binary peak lies in the $\phi_e = \pi$ half plane and the recoil peak lies in the $\phi_e = 0$ half plane. For this coordinate system, the FDCS can be expressed as $\sigma(\theta_p, \theta_e, \phi_e, E_e)$ since the projectile is in the $\phi_e = 0$ plane by definition. Although the cross sections depend on the observation angles of the projectile θ_p, it is customary to express the projectile polar scattering angle in terms of an equivalent parameter – the magnitude of the momentum transfer $\mathbf{Q}$.

The present 3C-HF results are compared with the absolute experimental measurements, the FBA-HF and 3C-169 in fig. 3 for 100 MeV/amu C^{6+} ionization of helium. For convenience, we plot results in the scattering plane in figs. 3-5 from zero to 360° which corresponds first to the $\phi_e = \pi$ half plane (zero to 180°) followed by the $\phi_e = 0$ half plane

(180° to 360°) with the angles being measured continuously clockwise relative to the beam direction. Although all the formulas are given for the CM system, the cross sections in the figures are presented for the laboratory system since this is the system of the experimental measurements. The conversion from CM to laboratory is a constant factor of 16 for the present FDCS. The momentum transfers of fig. 3 correspond to lab scattering angles of 0.7, 1.13, and 2.1 μrad respectively.

There are several important observations to be made from the results presented in fig. 3. First, both the experiment and theory have the same characteristic shape as one would expect from electron impact scattering with a binary peak (larger peak at 90°) and recoil peak (smaller peak at 270°). The binary peak results from a single two-particle projectile-electron collision and is located in the direction of the momentum transfer vector. The recoil peak is attributed to a double scattering mechanism in which the projectile first collides with the electron and then the electron back-scatters off the atomic nucleus. As can be seen from fig. 3, the recoil peak decreases rapidly with increasing momentum transfer (projectile scattering angle).

In Schulz et al. (2001), it was found that the shape of the 3C-169 results was in good agreement with the shape of the experimental data for all three momentum transfers displayed in fig. 3. Here we see that the 3C-169 (dashed curve) is about a factor of 3 smaller than the absolute data for all three cases. Both the FBA-HF (dotted curve) and 3C-HF (solid curve) results are in reasonable agreement with the absolute data for the two smallest momentum transfers with the 3C-HF being somewhat better. However, for the largest momentum transfer and largest ejected-electron energy, the FBA-HF and 3C-HF are almost the same and about a factor of 2 smaller than the data. For electron impact, the FBA-HF and 3C-HF results would be essentially identical for projectile-electron energies above about 1 KeV (speed of about 10 a.u.). The projectile speed for these experiments is about 60 a.u.! Here we see noticeable differences for the lower ejected-electron energies and smaller momentum transfers resulting from the larger charge of the projectile.

The experimental data presented in fig. 3 are averaged over finite bin sizes for both the energy of the ejected electron and the momentum transfer for the projectile while the theories were calculated at the centroid values. In fig. 4, 3C-HF results are presented that have been convolved over the experimental bin sizes (dashed curves). For the top part of the figure, the energy and momentum transfer convolution was for $(6.5\,eV \pm 3.5\,eV,\quad Q = 0.88 \pm 0.11)$, for the middle part of the figure $(17.5\,eV \pm 7.5\,eV,\quad Q = 1.43 \pm 0.22)$, and for the bottom $(37.5\,eV \pm 12.5\,eV,\quad Q = 2.65 \pm 0.44)$. It is seen that the convolution had a small effect on the results. Interestingly, the convolution slightly improved agreement between experiment and theory for the small momentum transfers where the agreement was already good and made it worse at the largest momentum transfer where the agreement with experiment is worst. Since the effect of convolution was small while dramatically increasing the computing cost, the remaining results in the paper will not be convolved.

Although HF wavefunctions have been used for some time now (Fainstein *et al*. 1994), it is still common practice to represent the initial and final states of the active electron as hydrogenic wavefunctions for some effective charge (Fiol *et al*. 2001, Olson and Fiol 2001). For helium, two different effective charges are typically used – 1.34 which yields the proper energy for ionizing the first electron and 1.69 which comes from minimizing the total energy for the helium atom. From fig. 3, it is seen that there is a significant difference in magnitude between using an effective charge of 1.69 (for both the bound and continuum state) and using HF bound states and static HF continuum states. Consequently, we decided to investigate the accuracy of effective charges further. In fig. 5, FBA results using different effective charges are compared with the FBA-HF results and experiment. When using effective charges, one has the choice of either using the same or different effective charges for the bound and continuum states. It can be argued that the same effective charge should be used for both states to ensure orthogonality of the active-electron wavefunction. As mentioned above, orthogonal active-electron wavefunctions cause the internuclear term to vanish. Further, if the wavefunctions are not orthogonal, additional shake-type amplitudes will be present which should be evaluated (Jones *et al*. 1992). FBA results are shown in fig. 5 obtained using an effective

charge of 1.34 for both the bound and continuum electron (chain curve) as well as 1.69 for both the bound and continuum electron (dashed curve). Recently, Olson and Fiol (2001) reported double differential cross sections for this process using an effective charge of 1.34 for the bound state and 1.0 for the continuum electron. FBA results (including the internuclear interaction) are also shown in fig. 5 for the effective charges of Olson and Fiol (2001) (dotted curve). Since the goal of the effective charges is to represent the helium atom and ion, the accuracy of the effective charges is determined by how well they reproduce the HF results (and not how well they reproduce the experiment!). From fig.5, it is clear that none of the choices for the effective charges are very accurate. An effective charge of 1.34 for both the bound and continuum electron fortuitously yields a better agreement with the experimental binary peak. On the other hand, the binary to recoil peak ratio is worse for this case. Since there is very little difference between the FBA-HF and 3C-HF results, our conclusion is that the HF approach is necessary for accurate results.

3.2 Out-of-Plane Results

In Schulz et al. (2001), it was noted that agreement between experiment and theory (at least shape agreement) was very good in the scattering plane but not as good in a plane perpendicular to the scattering plane, oriented such that it contains the beam direction. Consequently, we decided to investigate out-of-plane cross sections further. In the FBA, the cross sections are symmetric about the momentum transfer direction. As a result, according to the FBA, there should be no new information contained in any out-of-plane results. For the results shown in fig. 3, the momentum transfer direction is essentially at 90° (actually 89° to two significant figures) relative to the incident beam direction. Consequently, the FBA predicts that the cross sections in a plane perpendicular to the scattering plane and orientated such that it contains the momentum transfer direction should be the same as the in-plane results. 3C-HF cross sections in the scattering plane and in the plane perpendicular to the beam direction are compared with absolute experimental measurements in fig. 6 for ejected electrons with 6.5 eV and in fig. 7 for ejected electrons with 37.5 eV. The angular dependence of the perpendicular plane

results is the azimuthal angle ϕ_e. However, to make a direct comparison with the in-plane results, we define a new azimuthal angle $\beta_e = \phi_e - \frac{\pi}{2}$. Looking from the incident beam direction, $\beta_e = 0$ corresponds to straight up (y-axis), $\beta_e = \frac{\pi}{2}$ corresponds to the momentum transfer direction **Q**, $\beta_e = \pi$ corresponds to straight down (negative y-axis), and $\beta_e = \frac{3\pi}{2}$ corresponds to the x-axis. Since this perpendicular plane (nearly) contains the momentum transfer direction, the FBA predicts that the in-plane and out-of-plane cross sections should be the same. From fig. 6, it is seen that the agreement between experiment and theory is better in the scattering plane than it is in the perpendicular plane where the experimental data has a noticeably larger width for the binary peak. Also shown are the ratios of the cross sections in the two planes which would be (essentially) unity in the FBA. It is seen that the disagreement between experiment and theory is greatly enhanced in the ratio where the shape of the experiment and theory is almost opposite for both 6.5 eV and 37.5 eV! It should also be noted that another nice feature of the ratio is that it is independent of absolute values for the cross sections.

3.3 Integrated Cross Sections

We have seen that the experimental and theoretical FDCS are in satisfactory agreement in the scattering plane for 6.5 and 17.5 eV ejected electrons. On the other hand, fairly poor agreement was found for 37.5 eV ejected electrons in the scattering plane and serious problems were also found outside the scattering plane for all energies. The factor of two disagreement in the magnitude of the in-plane results at 37.5 eV was somewhat surprising since the shape of the experimental and theoretical results are in reasonable accord. It is of interest to see how the problems in the FDCS are reflected in less differential cross sections. First we examine a cross section integrated over the electron polar scattering angle and summed over two symmetric azimuthal angles

$$\sigma_4(\theta_p, \phi_e, E_e) = \int_0^{\pi} [\sigma(\theta_p, \theta_e, \phi_e, E_e) + \sigma(\theta_p, \theta_e, \phi_e + \pi, E_e)] \sin(\theta_e) d\theta_e \qquad (16)$$

This four-fold differential cross section depends on the azimuthal angle ϕ_e with $\phi_e \leq \frac{\pi}{2}$ (negative ϕ_e corresponds to below the scattering plane). The $\phi_e = 0$ results correspond to the integral of the scattering plane cross sections of fig. 3. By symmetry about the scattering plane, positive and negative angles must be identical.

Absolute experimental results for this integral are compared with 3C-HF and FBA-HF results in figs. 8-9 for 6.5 and 37.5 eV ejected electrons respectively. For 6.5 eV, the agreement between experiment and theory is very good except in the direction perpendicular to the scattering plane. For 37.5 eV., on the other hand, the agreement perpendicular to the scattering plane is good while the theory is about a factor of two smaller in the scattering plane (as would be expected from the in-plane FDCS results).

Doubly differential cross sections (DDCS) can be obtained by integrating over all possible emission angles of the ejected-electron plus the azimuthal angle for the projectile. Most of the DDCS work in the early years concentrated in cross sections integrated over all projectile scattering angles but here we are interested in cross sections differential in the polar scattering angle of the projectile and the ionized electron energy. Therefore we consider

$$\sigma^{DDCS}(\theta_p, E_e) = 2\pi \iint \sigma(\theta_p, \theta_e, \phi_e, E_e)\, d\Omega_e \qquad (17)$$

The 2π comes from the integration over the projectile azimuthal angle. In fig. 10, absolute experimental DDCS are compared with theory for the ejected-electron energies of figs. 8-9. Since there would be little difference between the 3C-HF and FBA-HF, only the FBA-HF results are shown as they are much easier to calculate. Instead of plotting the DDCS in terms of the projectile scattering angle (in micro-radians), it is more common to use an equivalent parameter – the momentum transfer perpendicular to the beam direction and this convention has been used for fig. 10. For the results presented here, the perpendicular component of the momentum transfer Q_{perp} and the momentum

transfer Q are the same to two decimal digits. The momentum transfer cross sections are given by

$$\sigma^{DDCS}(Q_{perp}, E_e) = \sigma^{DDCS}(\theta_p, E_e)\frac{\tan(\theta_p)}{K_f} \tag{18}$$

Recall that all the equations are for the CM system and the variables are CM quantities. One of the advantages of the momentum transfer cross section is that it is the same in both the center of mass and laboratory systems. The 6.5 eV results integrated over all ϕ_e emission angles of fig. 8 corresponds to one point in the top figure at 0.88 and the integral of the 37.5 eV results for fig. 9 lies at 2.65 in the bottom part of the figure. From Figs. 3 and 8, we see that the FDCS for 6.5 eV are in good agreement with experiment and here we see that the DDCS for the same momentum transfer is also in good agreement with experiment (within 1%). In a similar vein, the FDCS for 37.5 eV was approximately a factor of 2 smaller than experiment at the binary peak in fig. 3 and a factor of two smaller for angles near the scattering plane in fig. 9 and here this is reflected by the DDCS being lower than experiment for 37.5 eV electrons and a momentum transfer of 2.65. However, the ratio experiment/theory is reduced to 1.7. It is interesting that there is good agreement between experiment and DDCS theory for all small momentum transfers for 6.5 eV ejected electrons while the agreement is good only for a limited range of momentum transfers near 2.0 for 37.5 eV ejected electrons. Moshammer et al. (2001) and Olson and Fiol (2001) also presented DDCS for this process but at different ejected-electron energies. A visual comparison of the DDCS plots in those papers with the present results suggests that the present results are in better agreement with experiment. This evidently stems from the fact that both of the those calculations used effective charges for the bound and continuum states of the active electron. Disagreement at very small momentum transfers below about 0.7 a.u. will become significantly less pronounced if the theoretical results were convoluted with the experimental resolution in the transverse momentum transfer of about 0.2 a.u. (see the discussion in Moshammer et al. (2001)).

The next level of cross section to consider is the single differential cross section (SDCS). The SDCS is defined as

$$\sigma^{SDCS}(E_e) = \int \sigma^{DDCS}(\theta_p, E_e) \sin(\theta_p)\, d\theta_p \qquad (19)$$

Theoretical FBA-HF SDCS results are compared with absolute measurements in fig. 11. It is seen that there is excellent agreement between experiment and theory at 6.5 eV (4% difference) and theory is lower than experiment at 37.5 eV as one would have expected. However, now the difference between theory and experiment at 37.5 eV is only 11% which further illustrates the fact that detailed information about the collision is lost upon each integration. Finally the total cross section is the integral of the results of fig. 11 over energy. The integral for the theoretical cross sections is 1.44 x 10^{-17} cm^2 which is in very good agreement with the recommend value of 1.48 x 10^{-17} cm^2 by Rudd et al. (1985).

4. Conclusions

We have presented the first absolute measurements of the FDCS (fully differential cross section) for ion-atom ionization both in and out of the scattering plane. These measurements were compared with a 3C-HF calculation. The 3C-HF wavefunction is asymptotically an exact solution of the final-state effective three-body problem. In the past, theoretical treatments of ion-atom ionization, even if Hartree-Fock wavefunctions were used (Fainstein *et al*. 1994), have typically made a straight line approximation for the motion of the projectile and have neglected the projectile-nuclear interaction (Fainstein *et al*. 1991). Neither of these approximations is made in this work. Another advantage of the present approach is that a Hartree-Fock wavefunction is used for the initial state of the ejected electron and the final state is calculated numerically as an eigenfunction of the static Hartree-Fock potential for the ion. It has also been common to treat the initial and final states for the ejected-electron as an analytic Coulomb wave for some effective charge and the differences between using Coulomb and Hartree-Fock wavefunctions can represent factors of two or more.

It was found that the 3C-HF results were in very good agreement with absolute in-plane FDCS measurements for intermediate momentum transfer. For the largest momentum transfer, we found a factor of two difference between the magnitude of experiment and theory. This discrepancy becomes less pronounced when one looks at less differential cross sections and it is almost completely masked at the level of SDCS.

The out-of-plane results also indicated some substantial disagreement between experiment and theory. In the FBA, the FDCS is symmetric about the momentum transfer direction. According to the FBA, there is no new physics contained in the out-of-plane geometry and the cross sections in any plane containing the momentum transfer vector should be identical. We looked at two such planes – the scattering plane and a plane perpendicular to the incident beam which (nearly) contains the momentum transfer vector. For these two planes, the experimental data were noticeably different. Interestingly, the theoretical 3C-HF and experimental ratios of the cross sections for these two planes (predicted to be essentially unity in the FBA) exhibited an almost opposite behavior. This observation strongly suggests that the out-of-plane experimental results contain some physical effects not included in the theoretical approach.

The present theoretical approach is, in principle, a first order perturbation approach that contains many aspects of the problem to infinite order. The final-state 3C wavefunction individually contains the projectile-ion interaction, the projectile-electron interaction and the electron-ion interaction to infinite order. What is contained to first order is the initial-state projectile-ion and projectile-electron interaction. Consequently, it would be easy to argue that the discrepancy between experiment and theory must come from higher-order terms in the initial-state interactions. However, these interactions are contained in the CDW-EIS (continuum distorted wave with eikonal initial-state) approach and preliminary CDW-EIS calculations (with no other approximations) indicate that initial-state interactions will have very little effect on these results.

The important question then concerns the physics leading to the lack of agreement between experiment and theory for large momentum transfers and outside the scattering plane for a high-energy situation where one would have expected excellent agreement between experiment and theory. One plausible explanation for the lack of agreement outside the scattering plane is our reduction of the four-body problem to an effective three-body one. Note, however, that the FBA would be the same for any plane containing **Q** even if an exact helium wave function is used initially and finally. Thus, a higher-order theory in the projectile-atom interaction is needed to explain the out-of-plane data. On the other hand, a higher-order theory with a HF description of the target (3C-HF) does not reproduce the broadening of the binary peak observed in the plane perpendicular to the beam axis. Thus, *both* a higher-order theory *and* a better description of the helium atom are needed to explain the out-of-plane measurements. In contrast, the discrepancy in the scattering plane for larger momentum transfer could conceivably be resolved in the FBA by employing a better target description alone.

In summary, the present experimental results represent the first absolute FDCS measurements capable of obtaining cross sections in complete 3D-space. These results represent an exciting challenge to test theory at the most detailed level. Here we have seen that the 3C-HF approach is capable of explaining the in-plane intermediate momentum transfer results quantitatively and the high momentum-transfer results qualitatively. However, significant discrepancies were found outside the scattering plane which disappears upon comparison with successively less-differential cross sections.

Acknowledgements

The support of the NSF under grants PHY-0070872 and PHY-0097902, the Deutsche Forschungsgemeinschaft within the SBF 276, and the Leibniz-program, by GSI, the European Union and by CIRIL (GANIL at Caen) is gratefully acknowledged. Fruitful discussions with J. Fiol and R. E. Olson are acknowledged. We would like to thank W. Schmitt, H. Kollmus, R. Mann, R. Dörner, Th. Weber, K. Khayyat, A. Cassimi, L. Adoui,

J.P. Grandin and staff members of the CIRIL for their indispensable help performing the experiment at the GANIL.

References

Baertschy M D, 2002, in *Correlations, Polarization, and Ionization in Atomic Systems,* Ed. by D. H. Madison and M. Schulz, (American Institute of Physics, New York), p. 76.

Bencze G and Chandler C, 1999, Phys. Rev. A **59**, 3129

Berakdar J, Briggs J S, and Klar H, 1993, J. Phys. B **26**, 285.

Bethe H, 1930, Ann. Phys., Lpz. **5**, 325.

Brauner M, Briggs J S, and Klar H, 1989, J. Phys. B **22**, 2265.

Bray I, 1999, Phys. Rev. A **59**, 3133.

Bray I, 2000, J. Phys. B **33**, 581.

Bray I, Fursa D V, and Stelbovics A T, 2001, Phys. Rev. A **63**, 040702.

Bray I, Fursa D V, and Stelbovics A T, 2002, in *Correlations, Polarization, and Ionization in Atomic Systems,* Ed. by D. H. Madison and M. Schulz, (American Institute of Physics, New York), p. 90.

D A Biava, H P Saha, E Engel, R M Dreizler, R P McEachran, M A Haynes, B Lohmann, C T Whelan and D H Madison, 2002, J. Phys. B: At. Mol. Opt. Phys. **35**, 293-307.

Fainstein P D, Gulyás L, and Salin A, 1994, J. Phys. B **27**, L259.

Fainstein P D, Ponce V H and Rivarola R D, 1991, J. Phys. B 24, 3091.

Fang X, and Reading J F, 1991, Nuclear Instruments and Methods in Physics Research B **53**, 453.

Fiol J, Rodríguez V D and Barrachina R O,, 2001, J. Phys. B **34**, 933.

Fukuda H, Shimamura I, Vegh L, and Watanabe T, 1991a, Phys. Rev. A **44**, 1565.

Fukuda H, Watanabe T, Shimamura I and L. Vegh, 1991b, Nuclear Instruments and Methods in Physics Research B **53**, 410.

Gulyás L and Fainstein P D, 1998, J. Phys. B **31**, 3297.

Gulyás L, Fainstein P D, and Salin A, 1995, J. Phys. B 28, 245.

Haynes M and Lohmann B, 2001a, J. Phys. B **34**, L131.

Haynes M and Lohmann B, 2001b, Phys. Rev. A **64**, 044701.

Inokuti M, 1971, Rev. Mod Phys. **43**, 297.

Jones S and Madison D H, 1998, Phys. Rev. Lett. **84**, 2886.

Jones S and Madison D H, 2000, Phys. Rev. A **62,** 042701.

Jones S, Madison D H, and Srivastava M K, 1992, J. Phys. B **25**, 1899.

Madison D H and Shelton W N, 1973, Phys. Rev. A **8**, 2449.

Madison D H, Odero D O, and Peacher J L, 2000, J. Phys. B **33**, 4409.

Manson S T, Toburen L H, Madison D H, and Stolterfoht N, 1975, Phys. Rev. A **12**, 60.

Moshammer R, Fainstein P D, Schulz M, Kollmus H, Mann R, Hagmann S, and Ullrich J, 1999, Phys. Rev. Lett. **83**, 4721.

Moshammer R, Perumal A N, Schulz M., Rodríguez V D, Kollmus H, Mann R, Hagmann S, and Ullrich J, 2001, Phys. Rev. Lett. **87**, 223201.

Moshammer R, Ullrich J, Unverzagt M, Schmitt W, Jardin P, Olson R E, Mann R, Dörner R, Mergel V, Buck U, and Schmidt-Böcking, 1994, Phys, Rev. Lett. **73**, 3371.

Olson R E and Fiol J, 2001, J. Phys. B **34**, L625.

Rescigno T N, Baertschy M, Isaacs W A, and McCurdy C W, 1999, Science **286**, 2474.

Rodríguez V D and Barrachina R O, 1998, Phys. Rev. A **57**, 215.

Rudd M E, Kim Y -K, Madison D H and Gallagher J W, 1985, Rev. Mod. Phys. **57**, 965.

Rudd M E, Kim Y -K, Madison D H and Gay T, 1992, Rev. Mod. Phys. **64**, 441.

Salin A, 1989, J. Phys. B **22**, 3901.

Schulz M, Moshammer R, Madison D H, Olson R E, Marchalant P, Whelan C T, Walters H R J, Jones S, Foster M, Kollmus H, Cassimi A and Ullrich J, 2001, J. Phys. B **34,** L305.

Schulz M, Moshammer R, Perumal A N, and Ullrich J, 2002, accepted for publication in J. Phys. B.

Stelbovics A T, 1999, Phys. Rev. Lett. **83**, 1570.

Stolterfoht N, DuBois R D, and Rivarola R D, 1997, *Electron Emission in Heavy Ion-Atom Collisions* (Berlin: Springer).

Figure Captions

Figure 1. Jacobi coordinates used in the present work. The vector from the CM of the ion to the active electron is **r** and **R** is the vector form the CN of the ion-electron system to the projectile.

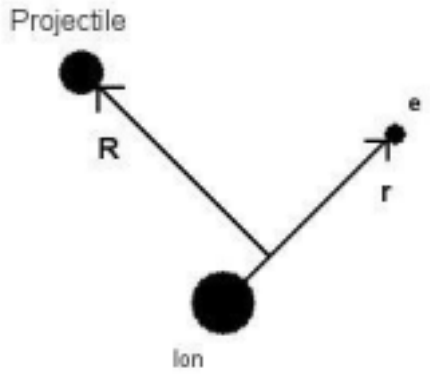

Figure 2 Spherical coordinate system used in the present work. The z-axis is parallel to the incident beam direction, the xz-plane is the scattering plane and the y-axis is perpendicular to the scattering plane.

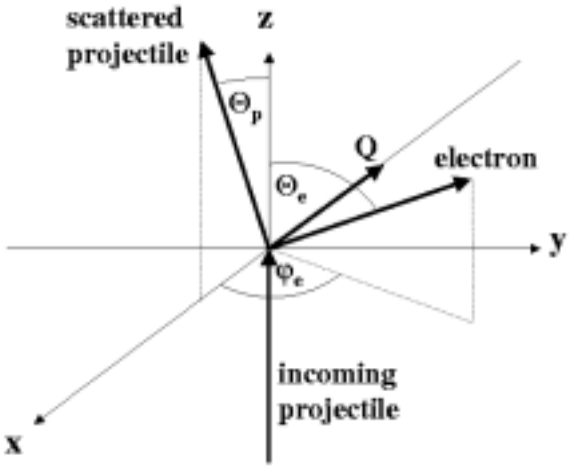

Figure 3. Scattering plane fully differential cross sections in the laboratory frame for 100 MeV/amu C^{6+} single ionization of helium. The energy of the ejected electron and the momentum transfer of the projectile is indicated in each part of the figure. The angle θ_e is the emission angle of the electron in the scattering plane measured clockwise from the beam direction. The solid circles are the present absolute measurements and the theoretical curves are: dashed – 3C-169; dotted – FBA-HF; and solid – 3C-HF.

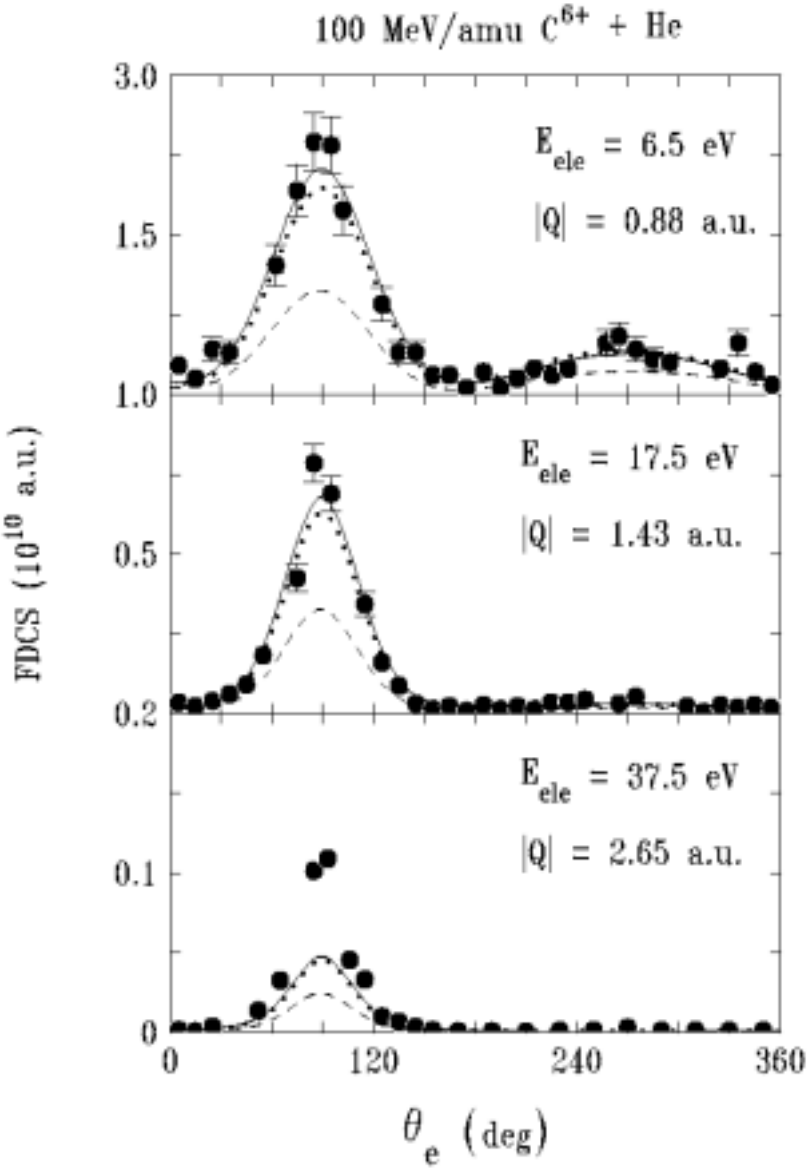

Figure 4. Same as fig. 3 except that the 3C-HF results have been convolved over experimental uncertainties in energy and momentum transfer. The solid circles are the present absolute measurements. The theoretical curves are: dashed – convolved 3C-HF and solid – 3C-HF.

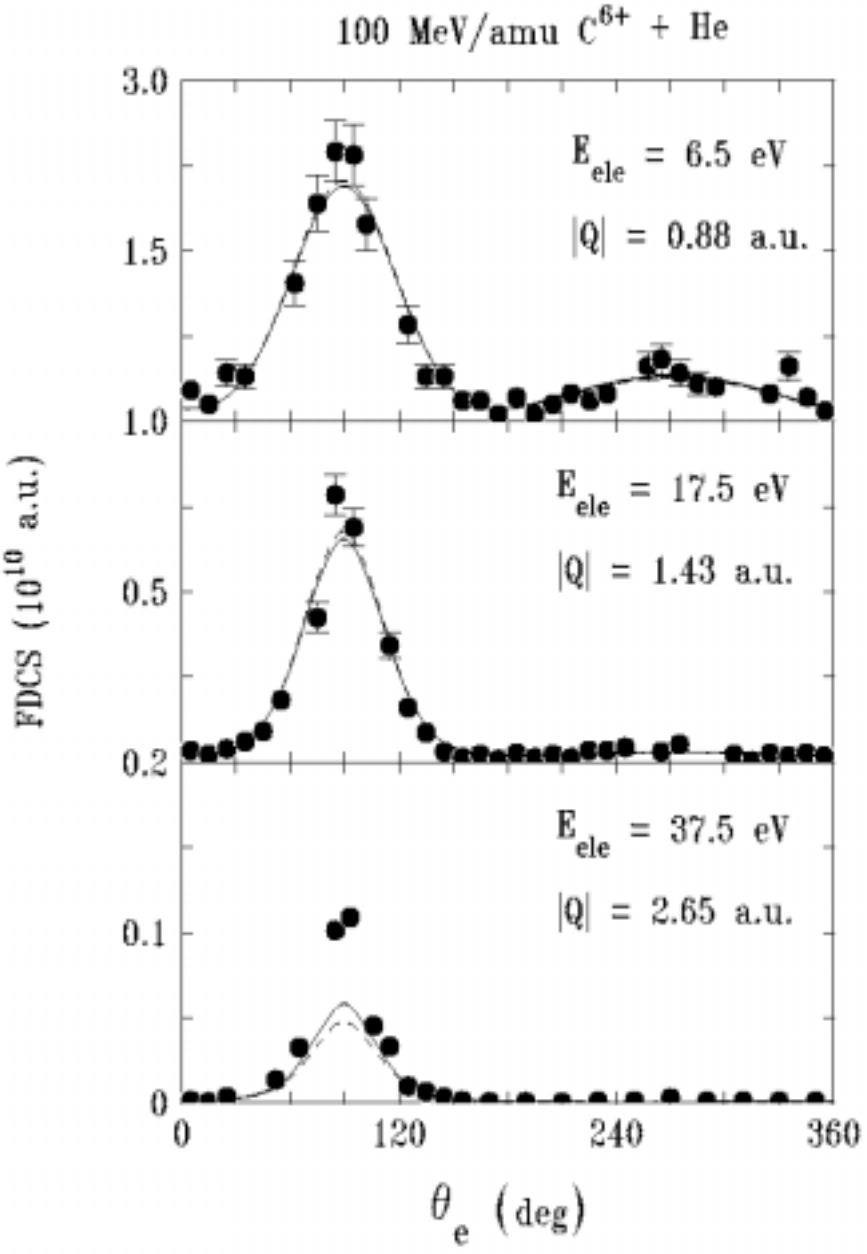

Figure 5. FBA fully differential cross sections in the laboratory frame using different wavefunctions for the active electron for 100 MeV/amu C^{6+} single ionization of helium. The energy of the ejected electron is 6.5 eV and the momentum transfer of the projectile is 0.88 a.u. The solid circles are the present absolute measurements and the theoretical curves are: solid – FBA-HF; dashed – FBA with hydrogenic bound and continuum wavefunctions for Z_{eff} = 1.69; chain - FBA with hydrogenic bound and continuum wavefunctions for Z_{eff} = 1.34; dotted – FBA with Z_{eff} = 1.34 for the bound state wavefunction and Z_{eff} = 1.0 for the continuum wavefunction.

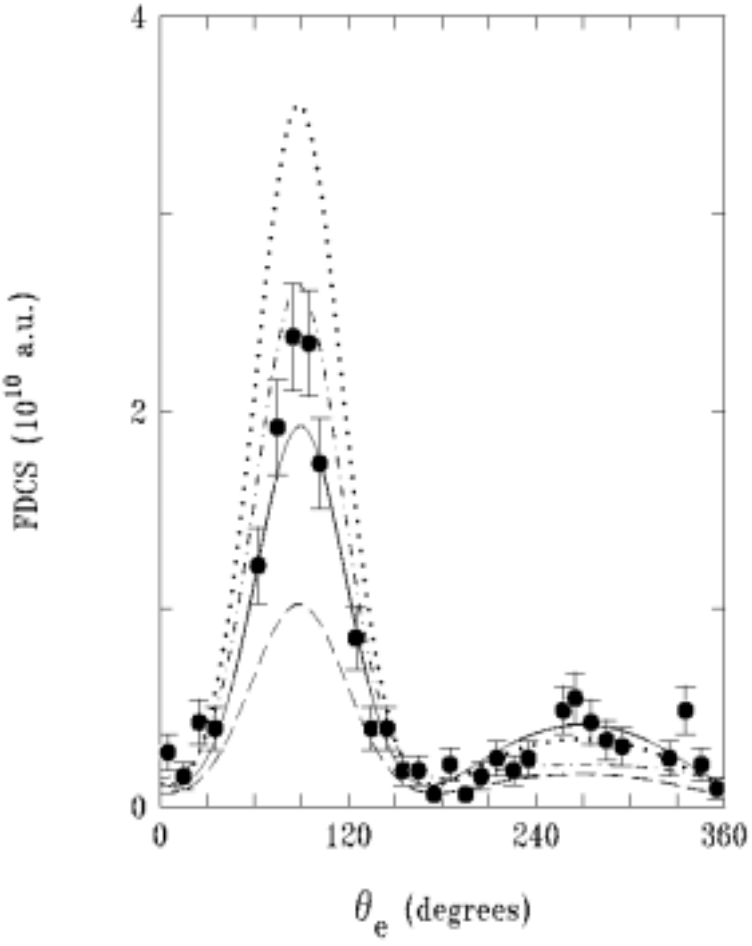

Figure 6. Comparison of in-plane and out-of-plane fully differential cross sections in the laboratory frame for 100 MeV/amu C^{6+} single ionization of helium. The top part of the figure corresponds to the in-plane FDCS depending upon the polar scattering angle θ_e. The middle part of the figure corresponds to a plane perpendicular to the incident beam direction and containing the momentum transfer vector **Q**. The angular dependence for the perpendicular plane is β_e. If the scattering plane is horizontal and one is viewing the collision from behind the incident beam, $\beta_e = 0$ in the perpendicular plane corresponds to straight up and $\beta_e = 90^\circ$ nearly corresponds to the location of the momentum transfer direction in the scattering plane (see text). The energy of the ejected electron is 6.5 eV and the momentum transfer of the projectile 0.88 a.u. The solid circles are the present absolute measurements the theoretical curves are the 3C-HF. The bottom part of the figure corresponds to the ratio of the results in the top figure and those in the middle figure

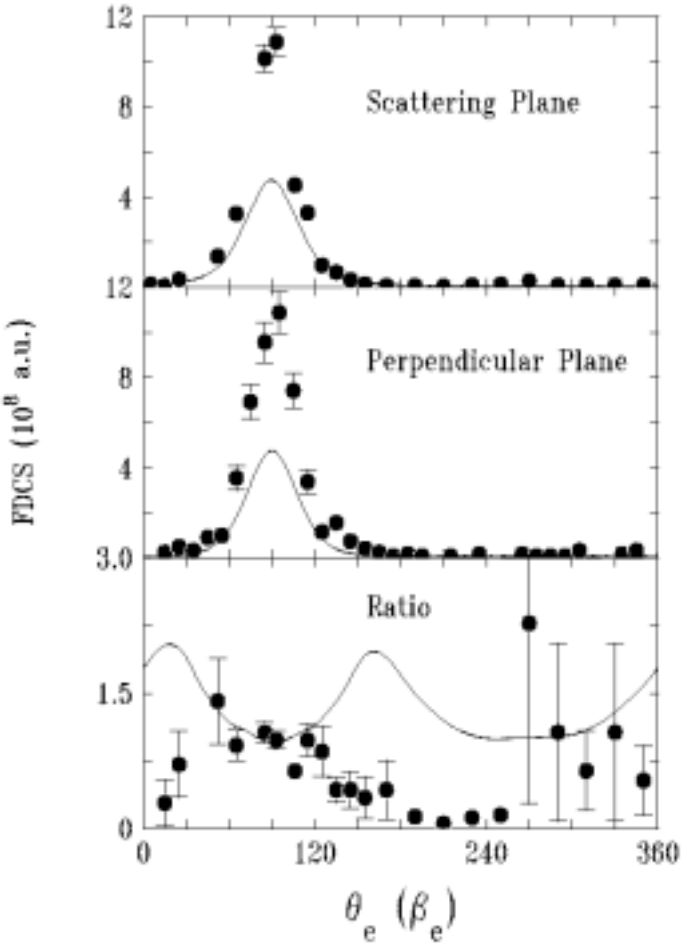

Figure 7. Same as fig. 6 except that the energy of the ejected electron is 37.5 eV and the momentum transfer of the projectile is 2.65 a.u.

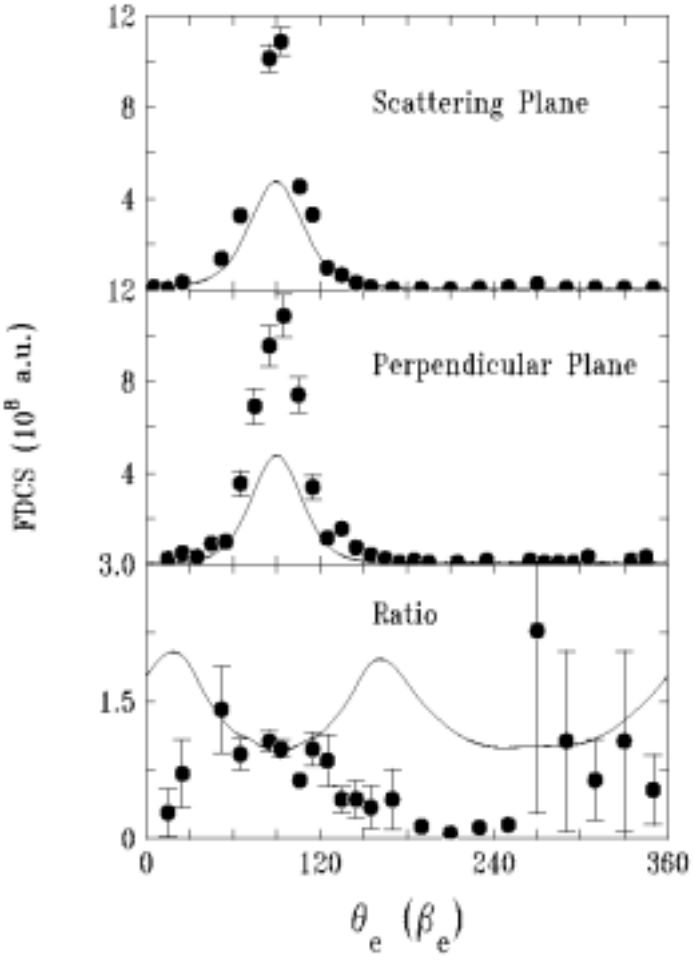

Figure 8. Integral of the laboratory FDCS over the polar emission angle θ_e of the ejected electron for 100 MeV/amu C^{6+} single ionization of helium (see Eq. 16). The scattering plane corresponds to $\varphi_e = 0^\circ$. Positive angles correspond to above the scattering plane and negative angles correspond to below the scattering plane. The cross section must be symmetric about the scattering plane. The energy of the

ejected electron is 6.5 eV and the momentum transfer of the projectile is 0.88 a.u. The solid circles are the present absolute measurements. The theoretical curves are: dotted – FBA-HF; and solid – 3C-HF.

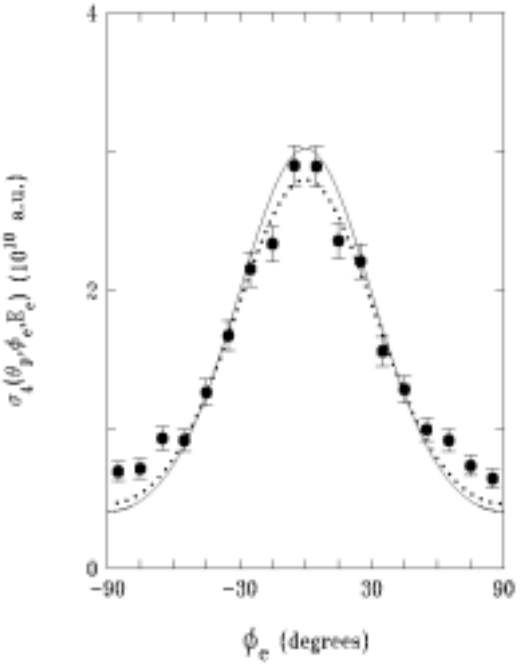

Figure 9. Same as fig. 8 except that the energy of the ejected electron is 37.5 eV and the momentum transfer of the projectile is 2.65 a.u.

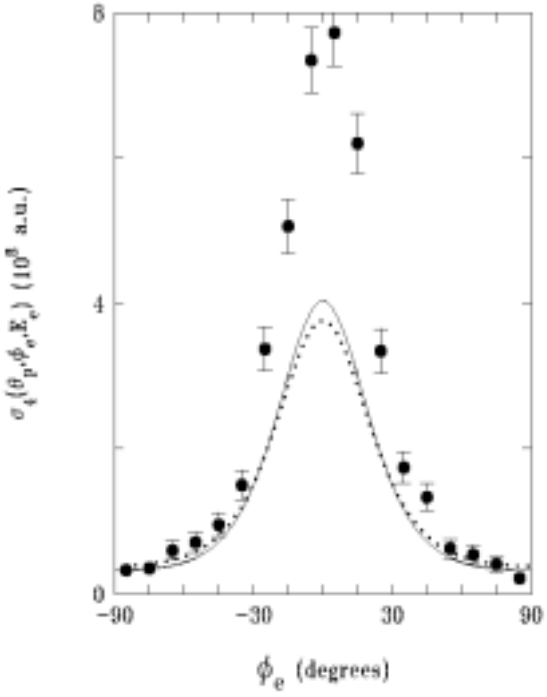

Figure 10. Double differential cross sections of Eq. (18) for 100 MeV/amu C^{6+} single ionization of helium in units of a_0^2/hartree/a.u.(Q_{perp}). Results are shown for two different ejected-electron energies indicated on the figure and the horizontal axis is the perpendicular component of the momentum transferred to the projectile. These cross sections are the same in the laboratory frame and the CM frame. The solid circles are the present absolute measurements and the theoretical curves are the FBA-HF.

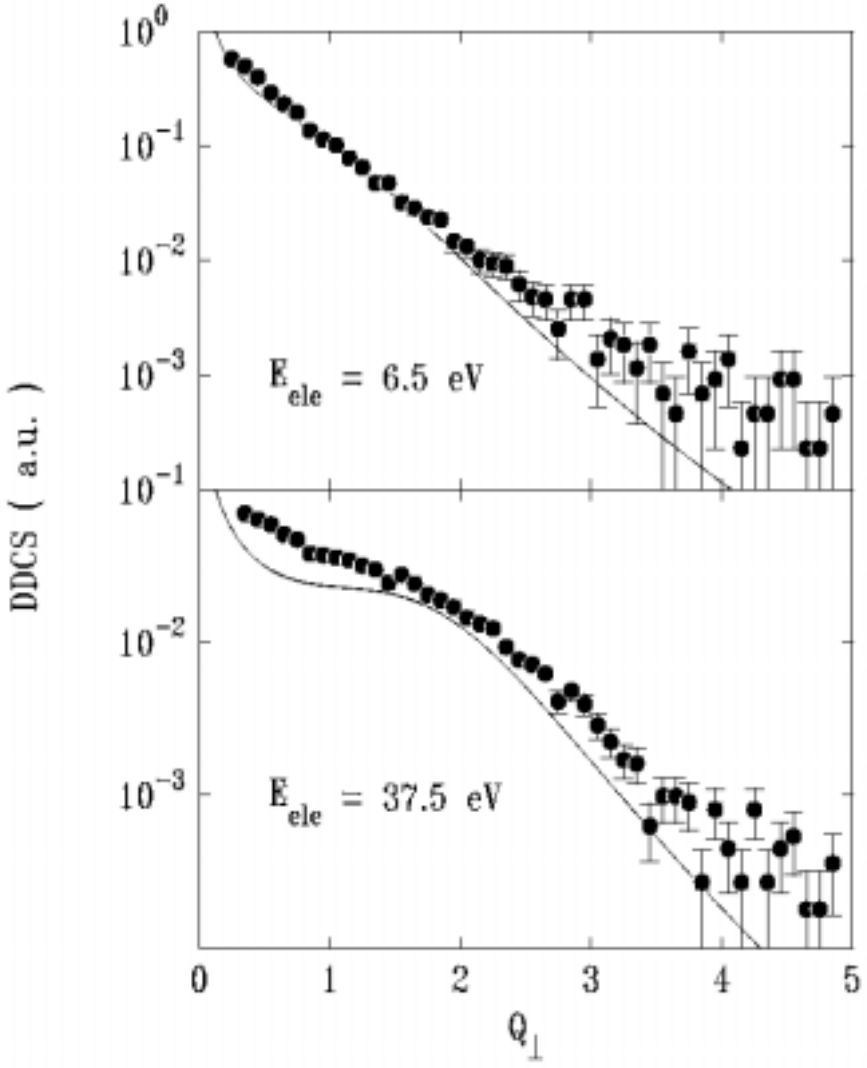

Figure 11. Single differential cross sections of Eq. (19) for 100 MeV/amu C^{6+} single ionization of helium. The horizontal axis is the energy of the ejected electron. The solid circles are the present absolute measurements and the theoretical curves are the FBA-HF.